Creation of Stable Poly(ethylene oxide) Surfaces on Poly(methyl methacrylate) Using Blends of Branched and Linear Polymers

D. G. Walton,† P. P. Soo, and A. M. Mayes*

Department of Materials Science and Engineering, Massachusetts Institute of Technology, Cambridge, Massachusetts 02139

S. J. Sofia Allgor, J. T. Fujii, and L. G. Griffith

Department of Chemical Engineering, Massachusetts Institute of Technology, Cambridge, Massachusetts 02139

J. F. Ankner and H. Kaiser

Research Reactor Center, University of Missouri—Columbia, Columbia, Missouri 65211

J. Johansson and G. D. Smith

Department of Chemical Engineering, University of Missouri—Columbia, Columbia, Missouri 65211

J. G. Barker and S. K. Satija

Reactor Radiation Division, National Institute of Standards and Technology, Gaithersburg, Maryland 20899

Received May 19, 1997; Revised Manuscript Received August 5, 1997[⊗]

ABSTRACT: Thin film miscible blends of poly(methyl methacrylate) (PMMA) and a branched random copolymer of methyl methacrylate and methoxy poly(ethylene glycol) monomethacrylate, P(MMA-*r*-MnG), were investigated by neutron reflectivity. The branched copolymer, which has a higher surface tension than PMMA, was nevertheless found to segregate to and completely cover both the surface and silicon substrate following annealing in 2000 Å thick films with ≥2 wt % P(MMA-r-MnG). This is in contrast to linear polyethylene oxide, which was depleted at both film interfaces when blended with PMMA and annealed. The reflectivity results were confirmed by contact angle studies, which indicate that the surfaces of P(MMA-*r*-MnG)/PMMA blends behave like that of pure P(MMA-*r*-MnG), resulting in a hydrophilic surface that is stable against dissolution in water-based environments. The branched hydrophilic additive is further shown to render PMMA resistant to protein adsorption and cell adhesion.

I. Introduction

In commercial applications it is often desired to modify polymer surfaces so as to promote such properties as adhesion, anti-fouling, biocompatibility, or wettability to paints, glues, and inks. Such characteristics have conventionally been achieved by employing chemical, flame, photochemical, and plasma treatments, as well as the grafting of moieties onto a surface, with the goal of modifying the surface's chemical composition, surface tension, or crystallinity in the near-surface region.[1,2] However, these traditional surface modification methods have the drawbacks of requiring extra processing steps and providing little control over the resulting nonequilibrium surface structure, which is then prone to reconstruction over time.

Another surface modification method uses preferential segregation of one component to the surface in multicomponent systems. This phenomenon is common to all materials classes and is typically driven by a reduction in the surface energy which more than compensates for the entropy decrease and/or energy increase associated with the demixing of the components. In polymer blends, this method is commonly employed with low molecular weight additives, but due to their small size, these additives can easily be removed from the surface by evaporation, dissolution, or wear. By using a polymeric additive, the segregating component is anchored to the matrix through entanglements, providing a more stable surface treatment. This method had been studied extensively both theoretically[3−11] and experimentally.[12−19]

Segregation has some distinct advantages over the traditional methods of surface modification. Because surface segregation is a thermodynamically driven process, the surface composition can be controlled and the resulting surface structure is in equilibrium. Moreover, additive segregation is an *in-situ* method, thus limiting the need for additional processing. It also allows the possibility of a "self-healing" surface, whereby removal of the segregating component would trigger further segregation from the bulk to replenish the surface.

Both energetic and entropic factors affect the segregation process. Cohesive energy differences between the components usually dominate, such that the lower energy component enriches the surface, reducing the material's surface tension. This was shown in early studies by Kramer and co-workers on blends of equivalent molecular weight polystyrene (PS) and deuterated polystyrene (PS-d_8), where the lower energy PS-d_8 enriched the surface.[12] Entropic effects are also important, however. For example, it is well-known that the degree of segregation increases as additive molecular weight decreases.[3,14,16,17] This effect can be large enough such that, in PS/PS-d_8 blends, PS will enrich the surface

† Current address: 3M, 3M Center, St. Paul, MN 55144.

⊗ Abstract published in *Advance ACS Abstracts,* October 15, 1997.

S0024-9297(97)00698-0 CCC: $14.00

when its molecular weight is much lower than that of its deuterated counterpart.[14]

Bond flexibility, or chain stiffness, is also thought to be an entropic factor influencing surface segregation. Klein and co-workers examined blends of chemically similar poly(ethylene-*r*-ethyl ethylene), P(E-*r*-EE), polyolefin random copolymers, where one component had a slightly higher EE content.[13] It was found that the surface was rich in this more branched species. Comparable results were found by Bates *et al.* with poly(ethylene propylene)-*b*-PEE diblock copolymers, where the block with the more branched PEE was observed to reside at the surface.[20] In each case, PEE has the smaller statistical segment length and is consequently more flexible than the other components. Using analytical SCF and functional theories, Fredrickson *et al.* proposed that this was the reason for PEE's localization at the surface.[4,11] From Monte Carlo (MC) simulations, however, Yethiraj and co-workers predicted that the stiffer component segregates preferentially to the surface due to better packing at the surface than in the bulk.[6,7] They suggested that the experimental results can be explained by the slightly lower surface tension of PEE.

Another entropic factor which is active in polymer systems is the tendency for chain ends to localize at the surface. In the vicinity of an interface, the total number of configurations available to polymer chains is reduced, and hence the entropy of the system. To minimize the number of "reflections" required by a polymer coil at the material boundary, chain ends preferentially segregate to the surface of a polymer melt, in the absence of strong interactions.[21−25] In one study by Affrossman *et al.*, triblock copolymers of PS with PS-d_8 tails and of PS-d_8 with PS tails *both* showed a large enhancement of chain ends at the substrate, indicating that this entropic effect is large enough to overcome the energetic difference between the blocks.[24] However, chemical modification of chain ends can strongly affect the degree of segregation. Elman *et al.* found that when carboxylic acid groups are attached to the end of PS chains, the high-energy ends are depleted at the surface.[25] Conversely, when PS is terminated by low-energy fluorocarbon tails, the ends enrich the surface. Similar results are found in polymer blends, where surface segregation of one component is enhanced by modifying its end groups.[17,18]

Recent theoretical studies[7,10,11] have addressed the question of whether branched polymers with a large number of chain ends blended with linear polymers might result in a high degree of surface segregation of the branched species, with the ultimate goal of segregating an energetically unfavorable component to the surface.[10] Using MC simulation, Yethiraj examined a blend of short, similar molecular weight branched and linear polymers.[7] For an athermal system, he predicted a depletion of the branched component from the surface. However, SCF results by other groups[10,11] predict a surface enhancement of the branched component based on configurational entropy arguments alone.

This paper builds on the theoretical work as well as recent experimental evidence[19] that segregation in blends of branched and linear polymers can be dominated by entropic considerations. Specifically, we demonstrate the surface segregation of a poly(ethylene oxide)- (PEO-) based branched polymer when blended with a lower energy poly(methyl methacrylate) (PMMA) matrix. The result holds particular interest as a means of creating stable hydrophilic surfaces. Like PEO, the branched additive, which consists of PEO branches randomly distributed along a PMMA backbone, exhibits good hydrophilicity—as does the surface of a *blend* between the additive and PMMA after annealing. Furthermore, the additive is shown to resist protein adsorption and cell adhesion, illustrating this system's potential importance for a range of applications in medical implants.[26,27]

Table 1. Physical Characteristics of Polymers

polymer	$\bar{M}_n$ [g/mol]	$\bar{M}_w/\bar{M}_n$	source
PMMA	330 000	1.11	Polysciences, Inc.
PMMA-d_8	222 000	1.01	(synthesized)
PMMA-d_8	314 000	1.06	Polymer Laboratories
PEO[a]	50 100	1.02	Polymer Laboratories
P(MMA-*r*-MnG)[b]	40 700	1.26	(synthesized)

[a] PEO terminated with methyl groups. [b] Copolymer 50% by mass each component.

II. Experimental Methods

Materials. The polymers used in this study were either purchased or synthesized by standard inert gas anionic polymerization techniques. Physical characteristics of each polymer are included in Table 1. Methyl methacrylate (MMA) monomer, purchased from Aldrich Chemical, was stirred and degassed over calcium hydride overnight. It was then vacuum distilled over calcium hydride at 60 °C, and the middle fraction was collected for use. Methoxy poly(ethylene glycol) monomethacrylate (MnG) macromonomer with approximately nine ethylene oxide units was purchased from Polysciences, Inc. The molecular weight of the macromonomer ($\bar{M}_n \sim 470$ g/mol) is too low for it to crystallize but too high for it to be readily distilled. Instead, the MnG was azeotropically dried with benzene three times on a vacuum line. LiCl (Aldrich) was dried *in vacuo* overnight at 130 °C. Five milliliters of each monomer were introduced to distilled tetrahydrofuran (THF) (refluxed over sodium benzophenone ketyl) at room temperature and then cooled to −45 °C. Ten milliliters of 0.098 M diphenylmethylpotassium in THF was then injected into the reactor. The dark red color of the initiator was replaced by a yellow-green which persisted throughout the synthesis. After 30 min, the reaction was terminated by injecting an excess of methanol, after which the solution turned colorless. The resulting random copolymer P(MMA-*r*-MnG) was 50% by mass of each component according to nuclear magnetic resonance (NMR) and had a molecular weight and polydispersity of $\bar{M}_n = 40\,700$ and $\bar{M}_w/\bar{M}_n = 1.26$ by gel permeation chromatography (GPC) and multi-angle laser light scattering (MALLS).

Deuterated methyl methacrylate (MMA-d_8) monomer, stabilized with 0.1% hydroquinone, was purchased from Cambridge Isotope Laboratories, Inc. After being stirred and degassed over calcium hydride, it was then vacuum distilled twice: first over calcium hydride at 55 °C and subsequently over trioctylaluminum (25% in heptane) at 55 °C. *sec*-Butyllithium (Aldrich, 0.15 M in cyclohexane) was titrated against an excess of 1,1-diphenylethylene and LiCl (to stabilize the carbanion) in distilled THF at −78 °C until a red-orange color persisted. An additional 240 μL of initator were then injected into the reactor, resulting in a deeper red color. Four grams MMA-d_8 were then added dropwise into the reactor, resulting in an immediate loss of color. The reaction was terminated with an excess of methanol after 60 min. The resulting PMMA-d_8 polymer had $\bar{M}_n = 222\,000$ and $\bar{M}_w/\bar{M}_n = 1.01$ by GPC/MALLS.

Sample Preparation. Additive and matrix polymers were codissolved in toluene at various blend concentrations. The solutions were filtered (Millipore GVHP013 0.2 μm filters) and then spin-coated (Headway Research, Inc. photoresist spinner 1-EC101DT-R790) onto polished silicon wafers (Exsil and Semiconductor Processing Co.) that had been cleaned for at least 1 day in chromic−sulfuric acid solution (Fisher Chemicals) and subsequently rinsed with deionized water (18.2 MΩ cm). Silicon wafers for neutron reflectometry were 10 cm in

diameter and 6 mm thick in order to prevent bending while being clamped for measurements. Films for contact angle and protein adsorption studies were made similarly on thinner (0.3−0.5 mm thick) silicon wafers, as were the films for cell adhesion experiments, which were spin-coated on standard microscope slides. Film thicknesses were measured by ellipsometry (Gaertner Scientific Corp. L3W26C.488.830) and samples were then annealed *in vacuo* for at least 5 days at 190 °C to achieve equilibrium and quenched to room temperature. For surface hydrophilicity experiments, samples were exposed to a humid environment of H_2O or D_2O for 2 weeks. A 95% humidity was achieved by enclosing the samples in a sealed glove box with a constant humidity solution of excess sodium sulfite in H_2O or D_2O at 20 °C. For small-angle neutron scattering (SANS) measurements, the polymers were coprecipitated and filtered. The blend in powder form was then melt-pressed at 200 °C in a 1.5 cm diameter, 3 mm thick ring.

Small-Angle Neutron Scattering. P(MMA-*r*-MnG)/PMMA-d_8 blends were studied with SANS performed on the Center for High Resolution Neutron Scattering (CHRNS) 30 m instrument at the Cold Neutron Research Facility (CNRF) at the National Institute of Standards and Technology (NIST) in order to determine the miscibility of the two polymers. A mechanical velocity selector with variable speed and pitch was used to obtain monochromated neutrons of wavelength $\lambda = 6.0$ Å and wavelength resolution $\Delta\lambda/\lambda = 0.15$. Scattered intensity was measured on a 65 cm × 65 cm ^{3}He position-sensitive proportional counter with 1 cm × 1 cm resolution, sample-to-detector distance of 8.1 m, and a beamstop of 5 cm, providing a wavevector q range of approximately 0.007−0.055 Å^{-1}. The sample was secured between two quartz windows in a brass enclosure which was connected to a temperature-controlled stage and maintained *in vacuo* during sample measurements. The sample was equilibrated at elevated temperatures *in situ* for 30 min before measurements began. Data were collected at each temperature with a sample aperture of 0.5 in. for 1 h, yielding on the order of 10^8 total monitor counts. The data were then corrected for background and empty cell scattering (using a similar sample holder without the polymer). Sample transmission was measured to be $T = 0.62$ and did not vary significantly with temperature. The relationship between the absolute scattering intensity and the detector counting rate was calculated from a silicon oxide standard (B2) provided by the Reactor Radiation Division at NIST. The scattering patterns were then circularly averaged since they were azimuthally symmetric.

A rigorous analysis of the SANS data would require the development of a new expression for the scattering function of a polymer blend consisting of homopolymer comprised of A segments and a random comb copolymer with a backbone comprised of A segments and randomly-spaced teeth made of B segments. Similar expressions have been constructed to describe the scattering from block copolymer/homopolymer blends.[28] More recently, Balazs and co-workers have published expressions for the scattering function of a random comb copolymer melt.[29,30] Their RPA analysis assumes that the segments comprising the teeth obey a Gaussian spatial distribution, strictly valid in the limit of long teeth. For our system, the teeth are short (∼nine ethylene oxide units), and the applicability of this approach is uncertain. While further examination of the scattering models used to describe comb polymer systems is of interest, it is beyond the scope of the present study. Here, we are primarily interested in confirming the miscibility of our two components, and the SANS data were therefore fit using the simpler random-phase approximation (RPA) model for a blend of homopolymers:[28,31]

$$\frac{1}{I(q)} = \frac{1}{[(b/V)_1 - (b/V)_2]^2}\left[\frac{1}{v_1\phi_1 N_1 P_1(q)} + \frac{1}{v_2\phi_2 N_2 P_2(q)} - \frac{2\chi}{(v_1 v_2)^{1/2}}\right] \quad (1)$$

where $I(q)$ is the scattered intensity, $(b/V)_i$, v_i, ϕ_i, and N_i are the scattering length density, the monomer volume, the volume fraction, and the degree of polymerization of component i, respectively, χ is the Flory−Huggins interaction parameter, and $P_i(q)$ is the normalized form factor given by the Debye formula for monodisperse random-coil polymers

$$P_i(q) = \frac{2}{(qR_{g,i})^4}\{\exp[-(qR_{g,i})^2] + (qR_{g,i})^2 - 1\} \quad (2)$$

where $R_{g,i}$ is the radius of gyration of component i. Values for PMMA-d_8 and P(MMA-*r*-MnG) are included in Table 2. Experimentally, the radius of gyration for P(MMA-*r*-MnG) is not known exactly, but is less than 100 Å from light scattering measurements. Thus R_g for P(MMA-*r*-MnG) and χ are fit for each sample, but the former must be constant across all measurements, such that when fit consistently, $R_g = 44$ Å. From the fitted data, the temperature dependence of χ can be fit to the relationship

$$\chi = A + \frac{B}{T} \quad (3)$$

where A and B are constants. While χ for PMMA/PEO blends has been shown to depend on the concentration of each component,[32] this effect was not analyzed in the present study.

Table 2. RPA Fitting Parameters

parameter	value	
	PMMA-d_8	P(MMA-*r*-MnG)
b/V	(see table 4)	
v (cm^3/monomer)	1.77×10^{-22}	1.83×10^{-21}[a]
ϕ	0.5	0.5
N	2907	41[a]
R_g (Å)	155	44

[a] Since P(MMA-*r*-MnG) is a random copolymer, it is actually misleading to talk about the monomer volume. In this case, however, the value is calculated from the polymer's density and molecular weight, so it represents an "average" value. The same is true for the degree of polymerization.

Table 3. Dispersion and Polar Surface Tension Components of Liquids

liquid	γ^d (dyn/cm)	γ^p (dyn/cm)
water	22.1	50.7
diidomethane	44.1	6.7
tricresyl phosphate	39.8	1.1

Contact Angle Measurements. Contact angle measurements (Advanced Surface Technologies, Inc. VCA2000) were performed with deionized water (18.2 MΩ cm), diidomethane (Alfa Æsar), and tricresyl phosphate (Alfa Æsar). The samples were raised toward a drop of fluid suspended from the tip of a syringe. Upon contact, the drop wets the sample. The sessile drop is then immediately captured with a video system, and the contact angle is measured. Given that the dispersion and polar components of the surface tension, γ^d and γ^p, respectively, for each fluid are known (Table 3), the surface tension of the sample can be derived from contact angle information using the harmonic-mean approximation to Young's equation[1]

$$(1 + \cos\theta_i)(\gamma_i^d + \gamma_i^p) = 4\left(\frac{\gamma_i^d\gamma_s^d}{\gamma_i^d + \gamma_s^d} + \frac{\gamma_i^p\gamma_s^p}{\gamma_i^p + \gamma_s^p}\right) \quad (4)$$

where θ_i is the contact angle of the sample measured with fluid i, and the subscript s denotes the polymer sample. The sample's surface tension is then calculated as the sum of its dispersion and polar surface tension components.

Neutron Reflectivity. Neutron reflectivity (NR) was performed on the grazing angle neutron spectrometer (GANS) at the Missouri University Research Reactor (MURR) in Columbia, Missouri[33] using monochromated neutrons with $\lambda = 2.35$ Å and $\Delta\lambda/\lambda = 0.015$, and on the IBM/UMINN/NIST reflectometer at the CNRF at NIST using monochromated neutrons with $\lambda = 4.768$ Å and $\Delta\lambda/\lambda = 0.025$. After background

Table 4. Polymer Scattering Length Densities

polymer	$10^6\ b/V$ (Å^{-2})	polymer	$10^6\ b/V$ (Å^{-2})
PMMA	0.98	PEO	0.63
PMMA-d_8	6.81	P(MMA-*r*-MnG)	0.49

subtraction and footprint correction at low angles, data were fit as described elsewhere.[34,35] For each of the control blends of PMMA and PEO, the concentration profile was modeled as a "single layer" with a hyperbolic tangent variation in the concentration at the surface and substrate interfaces. (In practice, this necessitates breaking the interfaces into a number of 5 Å slabs.) The use of tanh profiles for these systems is motivated by predictions from numerical self-consistent mean field (SCF) models of surface segregation in linear polymer blends.[3] For branched/linear polymer blends, SCF calculations predict more compact configurations of the segregated branched additives, with a slight maximum in the concentration profile close to the interface.[10,11] Thus as might be expected, the single layer model used for the linear control blends gave a poorer fit to data from the P(MMA-*r*-MnG)/PMMA systems.[10,11] Instead, a three layer structure was adopted to model volume fraction profiles for these systems, with error function interfaces between the layers. While more elaborate models might have been used to better characterize these systems,[11] we found in practice that the simple three layer model adequately described the data and captured the essential differences in the volume fraction profiles of segregating comb vs linear polymers.

From the model concentration profiles, a model scattering length density profile can be calculated, since the overall scattering length density $(b/V)_{tot}$ at any position in the sample is related to the component scattering length densities (b/V) by

$$(b/V)_{tot} = \sum_{i=1}^{n} \phi_i (b/V)_i \qquad (5)$$

The scattering length densities for each component (Table 4) were constrained to be equivalent across all systems. Theoretical reflectivities were calculated from the model $(b/V)_{tot}$ profiles using the Parratt formalism[36] and compared to the experimental data. The total film thickness, size of the near-surface regions, and width of the interfaces were adjusted until the calculated reflectivity converged with the measured data.

Protein Adsorption. Protein adsorption studies were performed to confirm the PEO-like nature of our blends and make an initial assessment of their utility as biomedical materials. Bovine serum albumin (BSA) adsorption measurements were made on 1 cm diameter, double-sided polished, 0.5 mm thick silicon wafers (Semiconductor Processing Co.) which were spin-coated with polymer films on both sides. The films were exposed to a mixture of unlabeled BSA (67 000 g/mol, globulin free, lyophilized, and crystallized, Sigma Chemical Co.) with ^{14}C-labeled BSA (American Radiolabeled Chemical Co.) in a buffered water solution (0.01M phosphate and 0.15M NaCl with pH = 7.0) and equilibrated by shaking for 6 h. Each sample's degree of radioactivity was then compared to that of the solution, from which the amount of BSA irreversibly adsorbed to the surface was determined.

Other protein adsorption experiments were performed on 1 in. × 1 in., 0.3 mm thick, double-sided polished silicon wafers (Semiconductor Processing Co.) prepared as before using human serum albumin (HSA, 68 000 g/mol, 5.440 mCi/mg) and equine cytochrome-*c* (ECC, 12 000 g/mol, 1.071 mCi/mg) (both from Sigma Chemical Co.). Samples were exposed to a mixture of ^{125}I-labeled and unlabeled proteins in a 0.01 M phosphate buffer solution (PBS, pH = 7.4). After 3.5 h, the samples were rinsed with saline solution and the degree of radioactivity associated with each surface was used to determine the amount of protein irreversibly adsorbed.

Cell Adhesion. Cell adhesion studies were additionally performed to assay bioinertness of the blend surface. Chinese hamster ovary (CHO) cells were suspended by trypsinization with 0.02% ethylene diamine tetraacetic acid (EDTA) and 0.25% trypsin in Hanks' balanced salt solution (HBSS), and collected by centrifugation. Cells were then resuspended in Dulbecco's modified Eagles medium (DMEM) containing 10% fetal bovine serum (FBS) and seeded onto sample films spin-coated on glass slides at a density of 10^5 cells/cm^2. After incubation at 37 °C in a humidified 10% CO_2 environment for 1.5 h, the samples were washed twice with the culture medium and observed by photomicrography. Samples were then returned to incubate and were again observed at 4 h.

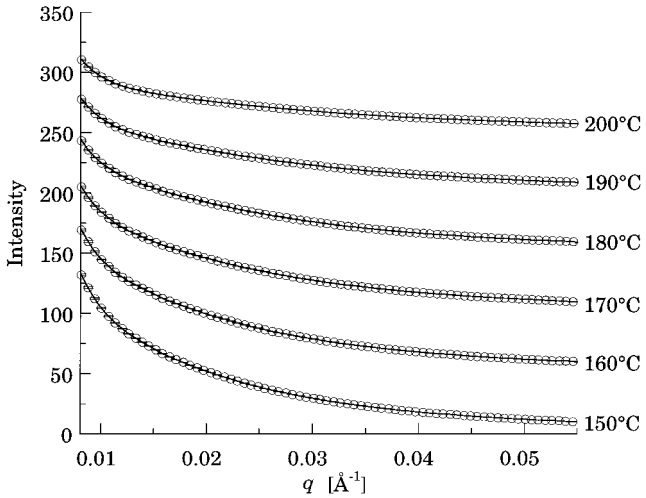

Figure 1. SANS data showing normalized intensity as a function of wavevector q for 50% blends by weight of PMMA-d_8 and P(MMA-*r*-MnG) at various temperatures, each offset by 50 for clarity. Data are fit (lines) to eq 1.

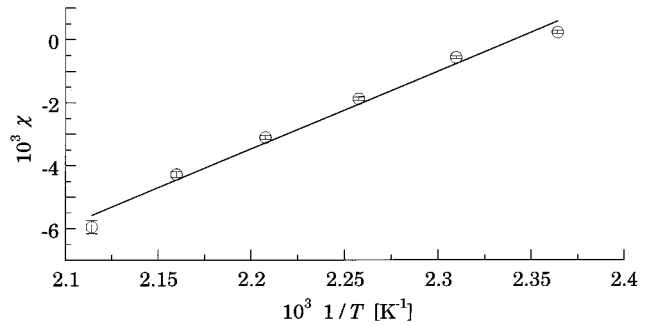

Figure 2. Flory−Huggins interaction parameter between PMMA-d_8 and P(MMA-*r*-MnG) as a function of temperature extracted from fits to the data in Figure 1.

III. Results and Discussion

Miscibility of P(MMA-*r*-MnG) and PMMA-d_8. SANS was performed on a 50% blend of 40 700 g/mol P(MMA-*r*-MnG) and 314 000 g/mol PMMA-d_8 in order to confirm their miscibility. Figure 1 shows the data, along with fits to the data after eq 1 using the parameters in Table 2. From the data at each temperature, a Flory−Huggins interaction parameter χ can be extracted, as shown in Figure 2. A fit to this data, following eq 3, leads to an interaction parameter of

$$\chi(T) = (-0.058 \pm 0.003) + \frac{(25 \pm 2)}{T} \qquad (6)$$

for this system (temperature is in Kelvin). As expected, this value is higher than the interaction parameter between PEO and PMMA-d_8,[32,37] but lower than that between PMMA and PMMA-d_8,[38] since P(MMA-*r*-MnG) contains both MMA and EO segments. At 190 °C, the temperature at which all samples were equilibrated, $\chi = -0.004$, indicating that the systems being studied are miscible blends.

Table 5. Contact Angle on Polymer Surfaces

	Contact Angle (deg)		
liquid	PMMA	PMMA-d_8	P(MMA-*r*-MnG)
water	70.7 ± 1.0	70.2 ± 1.0	70.8 ± 1.0[a]
diidomethane	42.8 ± 1.0	42.6 ± 1.0	35.6 ± 1.0
tricresyl phosphate	41.8 ± 1.0	42.1 ± 1.0	33.5 ± 1.3

[a] This value indicates the initial contact angle with water. The contact angle rapidly lowers as the surface absorbs water due to the PEO side chains (see Figure 9).

Table 6. Polymer Surface Tensions

	surface tension (dyn/cm)		
liquid pair	PMMA	PMMA-d_8	P(MMA-*r*-MnG)
water + diidomethane	43.9 ± 0.7	44.2 ± 0.7	46.1 ± 0.7
water + tricresyl phosphate	44.3 ± 0.7	44.4 ± 0.7	46.2 ± 0.8
diidomethane + tricresyl phosphate	42.5 ± 1.8	43.1 ± 1.4	45.6 ± 1.2
average	43.6 ± 1.1	43.9 ± 0.9	46.0 ± 0.9

Polymer Surface Tensions. Table 5 shows the contact angles of water, diidomethane, and tricresyl phosphate on 40 700 g/mol P(MMA-*r*-MnG), 330 000 g/mol PMMA, and 314 000 g/mol PMMA-d_8. Using eq 4 and various liquid pairs, the surface tension of each polymer was derived. Table 6 shows the results which indicate that P(MMA-*r*-MnG) is the higher-energy species. This suggests that any surface enhancement of P(MMA-*r*-MnG) when blended with either PMMA or PMMA-d_8 would be entropically-driven.

Segregation Studies. In these studies, control experiments on PEO/PMMA-d_8 blends were performed in order to compare the behavior of branched hydrophilic additives to linear hydrophilic additives. Previous studies have shown PEO and PMMA to be miscible.[32,37] It is also known that the surface energy of PEO is higher than that of PMMA-d_8.[1] From this, we would assume that the surface should be depleted with the higher energy PEO (*i.e.*, enhanced with PMMA-d_8). However, from contact angle measurements, Sakellariou found no enhancement of either component at the surface when 46 400 g/mol PEO was mixed in various concentrations with 100 000 g/mol PMMA.[39] In contrast to that study, in which samples were annealed for 3 h at 170 °C, all blends in our study were annealed for at least 5 days at 190 °C to achieve equilibrium. For the PEO/PMMA-d_8 blends specifically, samples were annealed at 190 °C for 2 weeks prior to measurement.

Figure 3 shows the NR data, taken at MURR, for blend films with thickness $L \sim 1000$ Å of 50 100 g/mol PEO in 222 000 g/mol PMMA-d_8 with 2, 5, 10, and 20% by weight of the PEO additive, each offset by a decade for clarity. Also presented are fits to the data obtained by assuming hyperbolic tangent concentration profiles[3] near the surface and substrate. The associated volume fraction profiles are shown in Figure 4, where the distance into the sample z has been normalized by the sample thickness L. Table 7 shows the thickness of each blend film as determined from the fits to the data and from ellipsometry and also compares the fitted total volume fractions to the original blend compositions.

These results show that in each sample the surface and substrate are depleted of PEO within approximately 50 Å from each interface. Additionally shown for the 20% blend in Figure 3 is a fit assuming a single layer system with no local concentration variation at the film interfaces (dotted line). The homogeneous film model gives a poorer fit to the data, overestimating the critical angle and the overall reflectivity. Also presented is a 20% blend of PEO and PMMA-d_8 which has not been annealed. This blend, which has not been allowed to relax toward equilibrium, shows no enhancement of either component. The unannealed sample also exhibits a higher surface roughness than the annealed films.

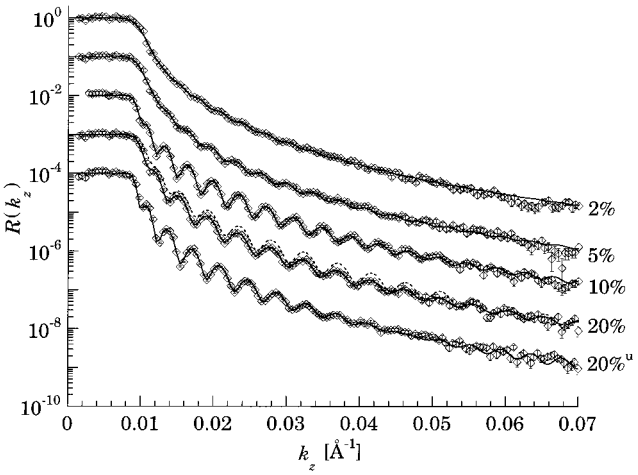

Figure 3. NR data (diamonds) and fits to that data (lines) for 2, 5, 10, and 20% by weight blend films of PEO in PMMA-d_8 as a function of wavevector k_z, each offset by a decade for clarity. Also shown is the reflectivity for a 20% blend film (denoted 20%^{u}) which is unannealed.

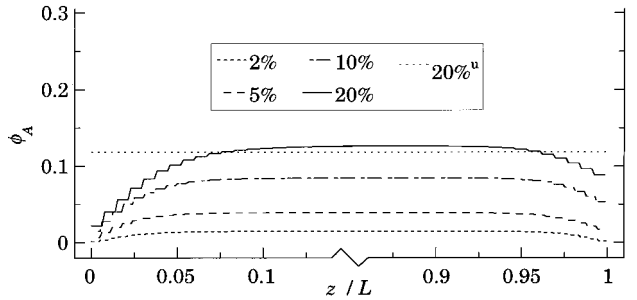

Figure 4. Volume fraction profiles of PEO, extracted from the fits to the data in Figure 3 after eq 5, as a function of the distance into the sample z, normalized by the sample thickness L, for the PEO/PMMA-d_8 blend films. Values for $0.15 < z/L < 0.85$ are omitted to emphasize the interfacial profiles.

Table 7. Fitted and Measured Values for PEO/PMMA-d_8 Blend Films

	ϕ_A		thickness (Å)	
%	fitted	measured	fitted	measured
2	0.01	0.02	936.5	950 ± 10
5	0.04	0.05	829.5	825 ± 7
10	0.08	0.09	798.7	810 ± 8
20	0.13	0.15	656.9	670 ± 10
20[a]	0.14	0.15	738.8	752 ± 53

[a] Unannealed sample.

Next, 1000 Å-thick blend films of P(MMA-*r*-MnG) with PMMA-d_8 are examined, where the branched additive is expected to be enthalpically driven away from the surface based on the components' surface tensions listed in Table 6. However, if a higher-energy component is branched, it might theoretically segregate to the surface for entropic reasons.[10,11] Figures 5 and 6 show the reflectivities and volume fraction profiles for 2, 5, 10, and 20% 40 700 g/mol P(MMA-*r*-MnG) blended in 314 000 g/mol PMMA-d_8 (measured at MURR). Complete segregation of the additive from the bulk to both interfaces is observed for all systems, such that

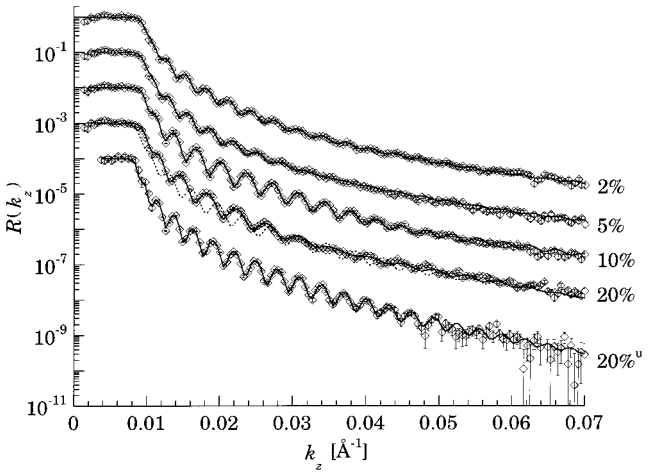

Figure 5. Experimental and theoretical reflectivities for thin film blends of 2, 5, 10, and 20% P(MMA-*r*-MnG) in PMMA-d_8 as a function of the wavevector k_z. Also shown is the reflectivity of an unannealed 20% blend film.

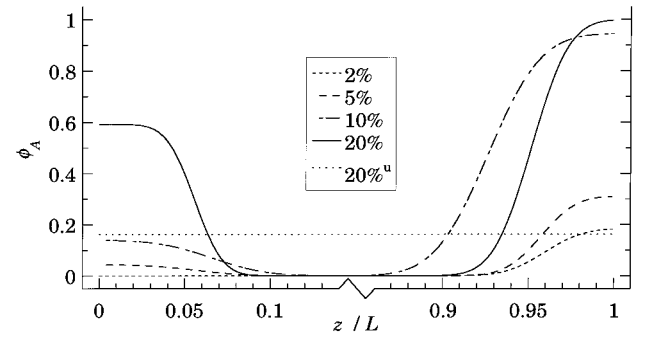

Figure 6. Volume fraction of P(MMA-*r*-MnG) in thin film P(MMA-*r*-MnG)/PMMA-d_8 blends as a function of reduced distance into the sample z/L. Values for $0.15 < z/L < 0.85$ are omitted to emphasize the interfacial profiles.

Table 8. Fitted and Measured Values for Thin Film P(MMA-*r*-MnG)/PMMA-d_8 Blends

	ϕ_A		thickness (Å)	
%	fitted	measured	fitted	measured
2	0.02	0.02	906.7	910 ± 10
5	0.04	0.06	885.8	890 ± 11
10	0.10	0.11	862.1	850 ± 9
20	0.19	0.21	769.2	760 ± 10
20[a]	0.20	0.22	989.3	1004 ± 48

[a] Unannealed sample.

the substrate is completely covered and the surface partially covered with P(MMA-*r*-MnG). For the 20% sample the surface coverage reaches 60%. The additive-rich regions adjacent to the surface and substrate have a thickness of approximately 50 Å, which corresponds to one additive radius of gyration (44 Å from Table 2). For these systems, the surface and substrate regions were better modeled as separate layers than with the hyperbolic tangent profiles commonly expected for linear polymer blends.[3] A more detailed analysis of these data using a "model-independent" fitting procedure[40,41] would be interesting to compare with SCF predictions of surface concentration profiles in branched/linear blends.[10,11] Table 8 shows good agreement between the fitted and measured thicknesses and between measured and fitted total volume fractions. As shown in Figure 6 for the 20% blend (dotted line), a homogeneous film model underestimates the critical edge and fails to capture the oscillation period. The unannealed sample shows, as before, no enhancement of either component at the interfaces.

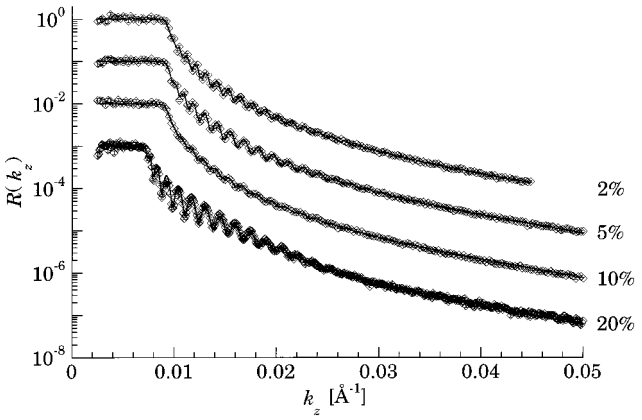

Figure 7. Experimental and theoretical reflectivities for thick film blends of 2, 5, 10, and 20% P(MMA-*r*-MnG) in PMMA-d_8 as a function of the wavevector k_z.

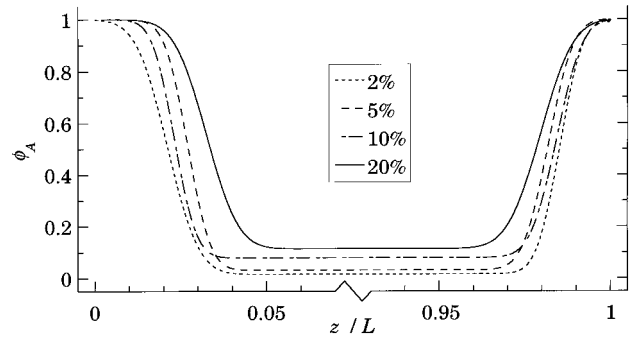

Figure 8. Volume fraction of P(MMA-*r*-MnG) in thick film P(MMA-*r*-MnG)/PMMA-d_8 blends as a function of reduced distance into the sample z/L. Values for $0.075 < z/L < 0.925$ are omitted to emphasize the interfacial profiles.

Table 9. Fitted and Measured Values for Thick Film P(MMA-*r*-MnG)/PMMA-d_8 Blends

	ϕ_A		thickness (Å)	
%	fitted	measured	fitted	measured
2	0.03	0.02	2280.0	2300 ± 25
5	0.08	0.06	1986.7	1980 ± 19
10	0.12	0.10	2002.3	2019 ± 13
20[a]	0.18	0.19	1971.3	1951 ± 15

[a] Reverse geometry used.

Since the additive is completely depleted from the interior of the 1000 Å-thick blend films on annealing, one would expect that thicker films, with smaller surface to volume ratios, should exhibit a higher percentage of additive at the surface. This is verified by the reflectivities and volume fraction profiles of $L \sim$ 2000 Å P(MMA-*r*-MnG)/PMMA-d_8 blend films (measured at NIST)[42] as shown in Figures 7 and 8 and in Table 9, where again the near-surface and -substrate regions are modeled as separate layers. Both film interfaces exhibit a monolayer coating ($\sim R_g$ thick) of the branched component for all blend compositions, without significant depletion of the additive from the bulk. From this result one can rule out a surface-induced phase separation of the blend components. Moreover, the degree of segregation observed is much higher than what is expected on the basis of molecular weight differences alone.[38,43] The results thus provide evidence for the surface segregation of a higher energy component based on molecular architecture.

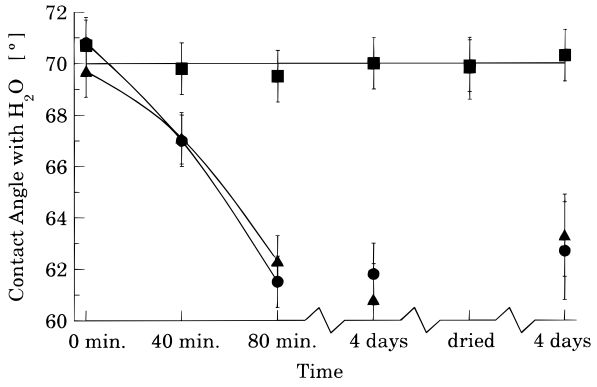

Figure 9. Contact angle as a function of time immersed in water of PMMA (■), P(MMA-*r*-MnG) (●), and a blend film of 20% P(MMA-*r*-MnG) in PMMA (▲).

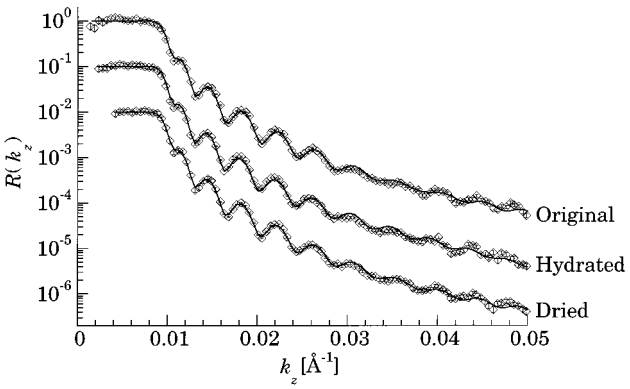

Figure 10. Experimental and theoretical reflectivities as a function of the wavevector k_z for a 20% blend film of P(MMA-*r*-MnG) in PMMA-d_8 for initial, H_2O hydrated, and dried states.

Surface Hydrophilicity. In order to determine the surface hydrophilicity of the P(MMA-*r*-MnG)/PMMA blends, a 20% blend film of 40 700 g/mol P(MMA-*r*-MnG) in 330 000 g/mol PMMA with thickness $L \sim 2000$ Å was immersed in deionized water (18.2 MΩ cm) for a specified amount of time. The sample was then removed from the water and contact angle measurements were immediately taken. The results were then compared to pure P(MMA-*r*-MnG) and PMMA, which were prepared similarly. The NR results in Figure 7 for a blend film with similar thickness indicate the surface is completely covered with the branched additive. Thus it is expected that since PEO is hygroscopic, if the PEO side chains of the branched additive are located at the surface, then the contact angle will decrease as water is absorbed into the system. The results shown in Figure 9 indicate, as expected, that the contact angle over PMMA does not change as a function of immersion time in water. For both pure P(MMA-*r*-MnG) and the P(MMA-*r*-MnG)/PMMA blend, however, the contact angle decreases sharply over the first 80 min as the sample absorbs water and then stabilizes approximately 10° lower than its initial value, remaining unchanged after 4 days of immersion. Subsequent drying and rehydration provides similar results indicating reproducible behavior.[43] The contact angle drop over the P(MMA-*r*-MnG)/PMMA blend provides more evidence that the higher energy P(MMA-*r*-MnG) is located at the surface, and the fact that its final contact angle is the same as pure P(MMA-*r*-MnG) indicates that their surfaces are chemically similar. Also, the reproducibility of the results indicates that immersion in water does not remove P(MMA-*r*-MnG) from the surface. Thus, even though PEO is water-soluble, the PMMA backbone effectively anchors the branched additive, and consequently the PEO side-chains, to the PMMA matrix.

Although promising, the data shown in Figure 9 raise some questions. The first is why does the branched copolymer surface take 80 min to hydrate when PEO wets almost instantaneously? This is not surprising, however, when one recognizes that the presence of a PMMA backbone, which helps anchor the additive to the matrix, hinders water's ability to interact with the PEO side-chains. In support of this hypothesis, Shard *et al.* have recently shown, using X-ray photoelectron spectroscopy (XPS) and static secondary ion mass spectrometry (SSIMS), that in a similar copolymer with longer PEO branches, the PMMA backbone is found near the surface and the methyl-group-terminated branch ends localize at the surface.[44] This causes partial shielding of the PEO side chains from the surface and restricts their expansion into water. Another question is how a surface that exhibits a 60° contact angle with water can be termed hydrophilic. It may be argued that since water does not completely wet the P(MMA-*r*-MnG) surface, (*i.e.*, the contact angle is not 0°) that the surface is not hydrophilic. However, this traditional view of what defines hydrophilicity has recently come under review.[2,45] For example, poly(hydroxy ethyl methacrylate) (PHEMA), which is the main constituent of soft contact lenses and is considered to be hydrophilic, also exhibits a contact angle with water of about 60°. This is thought to be due to the hydrophobic methyl groups on the chain ends which preferentially localize at the surface, as previously mentioned, and partially screen the hydrophilic nature of the polymer below the surface. This situation is also present with P(MMA-*r*-MnG) where the side chains are also methyl-group-terminated. A better way to identify the hydrophilicity of polymers such as these is to analyze the equilibrium water content, which, for PHEMA, is 40%.[2]

In order to determine the equilibrium water content of the P(MMA-*r*-MnG)/PMMA blend surfaces, 1000 Å thick films of 20% 40,700 g/mol P(MMA-*r*-MnG) blended in either 330 000 g/mol PMMA or 314,000 g/mol PMMA-d_8 were exposed to a humid environment of H_2O or D_2O for 2 weeks, as described earlier. Neutron reflectivity on these hydrated samples were then compared to data taken on the samples prior to hydration and after subsequent drying in a vacuum oven overnight.

Unlike the NR measurements already presented, in this case the system consists of 3 components, complicating the reduction of the fitted scattering length density profiles to volume fraction profiles. Even though the scattering length densities of all components are known (Table 4), and the volume fraction of all 3 components sum to unity, there are still two unknown quantities. This problem is overcome by examining absorbed H_2O in a blend of the branched additive with PMMA-d_8 and comparing the results to a system of absorbed D_2O in a blend of the additive with PMMA. The effects of deuteration on the concentration profile should be negligible, yielding two independent measurements of the system. This allows one to back out a volume fraction profile that describes both.

Figures 10 and 11 show the reflectivities and scattering length density profiles for a 20% blend of 40 700 g/mol P(MMA-*r*-MnG) in 314 000 g/mol PMMA-d_8 before and after hydration with H_2O, along with the redried data. The scattering length density profiles indicate

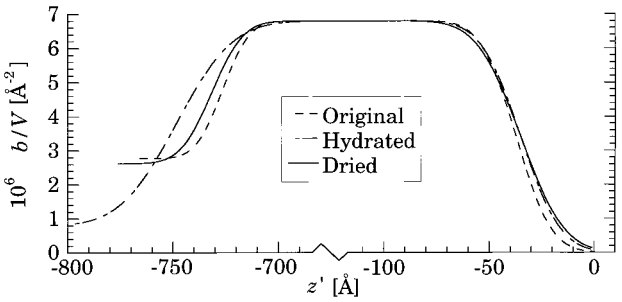

Figure 11. Scattering length density profiles for P(MMA-*r*-MnG)/PMMA-d_8 blend film in initial, H_2O hydrated, and dried states as a function of distance into the sample z'. Values for -675 Å $< z' < -125$ Å are omitted to emphasize the interfacial profiles.

Table 10. Fitted and Measured Values for P(MMA-*r*-MnG)/PMMA-d_8 Blend Films Hydrated With H_2O

	thickness (Å)	
state	fitted	measured
original	769.2	760 ± 10
hydrated	804.0	
dried	776.0	

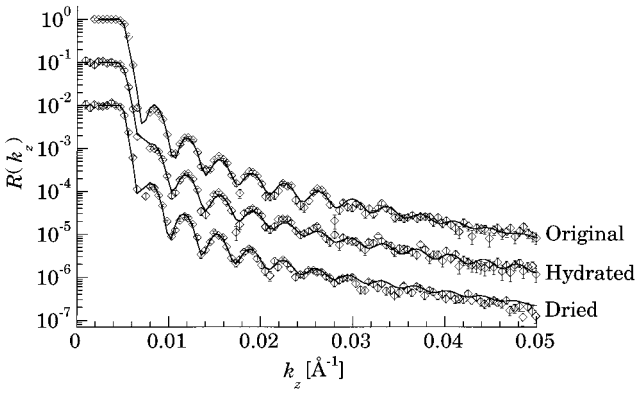

Figure 12. Experimental and theoretical reflectivities as a function of the wavevector k_z for a 20% blend film of P(MMA-*r*-MnG) in PMMA for initial, D_2O hydrated, and dried states.

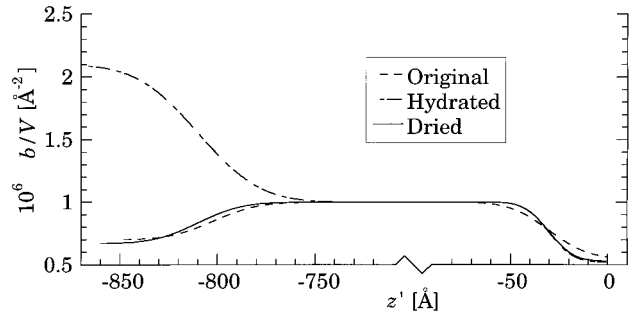

Figure 13. Scattering length density profiles for P(MMA-*r*-MnG)/PMMA blend films in initial, D_2O hydrated, and dried states as a function of distance into the sample z'. Values for -700 Å $< z' < -100$ Å are omitted to emphasize the interfacial profiles.

that the original and dried states are similar, whereas the hydrated state's near-surface region not only has a lower scattering length density but also is expanded from the sample's dried state, resulting in a sample thickness increase of approximately 30 Å (Table 10). Figures 12 and 13 show the results for a similar blend with 330,000 g/mol PMMA hydrated with D_2O. Again, the original and dried states are similar while the hydrated state shows a marked difference in the near-surface region and a larger sample thickness (Table 11). The scattering length density profiles of the hydrated states in Figures 11 and 13 were iterated upon such that best fits were achieved with a single volume fraction profile (shown in Figure 14) describing both systems. This volume fraction profile shows H_2O or D_2O only in the near-surface region, with an equilibrium water content of 27% at the surface, similar to, but lower than, that of PHEMA. The measured equilibrium water content corresponds to approximately three water molecules per ethylene oxide unit in the additive's side chains, which agrees with published results that state that from one to three water molecules can coordinate each ethylene oxide segment.[46,47]

Table 11. Fitted and Measured Values for P(MMA-*r*-MnG)/PMMA Blend Films Hydrated With D_2O

	thickness (Å)	
state	fitted	measured
original	851.8	830 ± 15
hydrated	872.8	
dried	859.8	

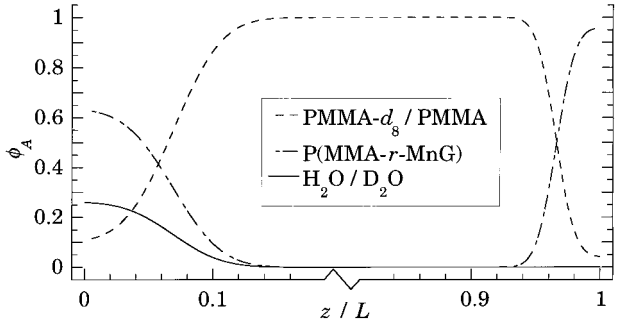

Figure 14. Volume fraction profile for P(MMA-*r*-MnG)/PMMA-d_8 or P(MMA-*r*-MnG)/PMMA blend films hydrated with H_2O or D_2O as a function of reduced distance into the sample z/L. Values for $0.2 < z/L < 0.8$ are omitted to emphasize the interfacial profiles.

Table 12. Irreversible Protein Adsorption on Sample Surfaces

	amount adsorbed (μg/cm^2)		
protein	PMMA	P(MMA-*r*-MnG)	20% blend
BSA	1.2 ± 0.04	0.02 ± 0.08	0.53 ± 0.05[a]
HSA	0.717 ± 0.004	0.021 ± 0.004	0.018 ± 0.003
ECC	10.35 ± 0.04	0.14 ± 0.005	0.15 ± 0.005

[a] Blend surface ~60% coated with P(MMA-*r*-MnG).

Protein Adsorption and Cell Adhesion. PEO is not only hydrophilic, but is also a polymer that resists protein adsorption and cell adhesion.[26,47−49] Thus the PEO-based P(MMA-*r*-MnG) and the surfaces of PMMA/P(MMA-*r*-MnG) blends, which were shown to be hydrophilic, are good candidates for controlling the interactions of polymer surfaces with biological fluids. These systems have commercial relevance since PEO and PMMA are both components of many FDA approved implantable devices. In order to study the bioinert nature of P(MMA-*r*-MnG), protein adsorption and cell adhesion experiments were performed on films of 330 000 g/mol PMMA, 40 700 g/mol P(MMA-*r*-MnG), and a 20% blend of P(MMA-*r*-MnG) in PMMA, prepared as before.

Table 12 shows the results of BSA adsorption experiments on 1000 Å thick polymer films. The P(MMA-*r*-MnG)-enriched PMMA surface shows roughly half the amount of protein adsorption as pure PMMA, while pure P(MMA-*r*-MnG) effectively inhibits all protein adsorption. The degree of BSA adsorption for the film with

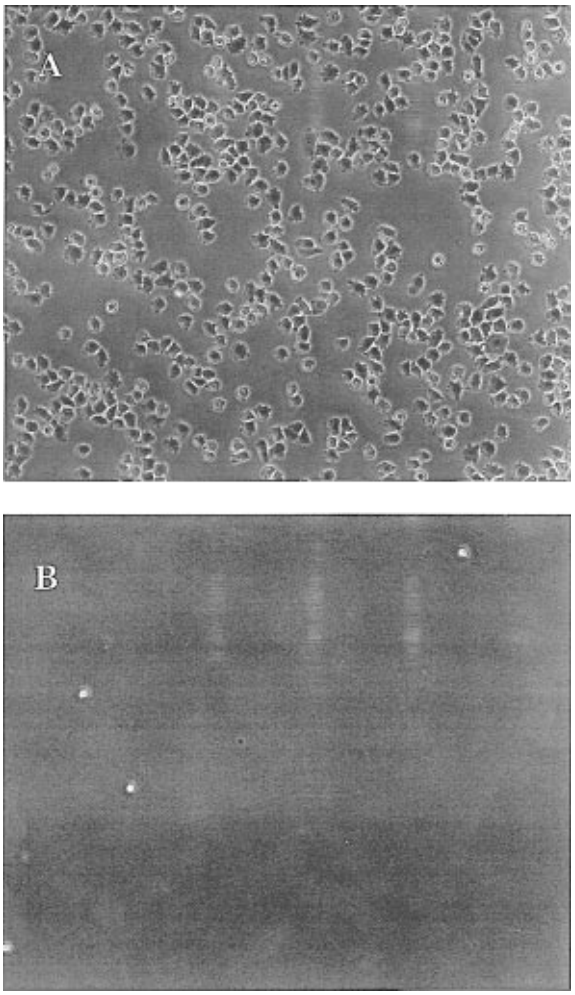

Figure 15. CHO cell adhesion on (A) PMMA after 4 h and (B) P(MMA-*r*-MnG)-enriched PMMA after 4 h.

20% P(MMA-*r*-MnG) is consistent with the 60% additive surface coverage for blend films of this concentration and thickness shown by neutron reflectivity (Figure 6).

For thicker blend films, complete coverage of the surface by the branched copolymer additive should yield higher degrees of protein adsorption resistance. Table 12 additionally shows results of HSA and ECC protein adsorption experiments on 2000 Å thick films. The protein adsorption resistance was examined using these two proteins with different molecular weights in order to compare results with a recent study which finds that with grafted PEO surfaces, lower molecular weight proteins need higher grafting densities to effectively resist protein adsorption.[49] Here, though, irrespective of molecular weight, both pure P(MMA-*r*-MnG) and P(MMA-*r*-MnG)-enriched PMMA surfaces almost completely inhibit protein adsorption compared to the pure PMMA samples, indicating that the surface of a P(MMA-*r*-MnG)/PMMA blend does, indeed, resemble pure P(MMA-*r*-MnG) as shown by neutron reflectivity.

Since cells adhere via the attachment of proteins, the fact that these surfaces resist protein adsorption implies that they should also resist cell adhesion.[50] In order to test this, CHO cells were seeded onto sample films with thickness $L \sim 2000$ Å. Figure 15A shows that CHO cells have spread substantially on PMMA after 4 h. In contrast, the P(MMA-*r*-MnG) surfaces at 4 h show little cell adhesion and no spreading. Similar results are seen with the P(MMA-*r*-MnG)/ PMMA blend surfaces at 4 h (Figure 15B), again providing evidence that the surface of the blends resembles pure P(MMA-*r*-MnG).

Conclusions

In this paper, evidence supporting the entropically-driven segregation of a higher-energy additive to the surface of a polymer blend due to architectural modification of the additive is presented. Using neutron reflectivity, it is shown that while linear PEO segregates away from the surface in blends with PMMA-d_8 on annealing, the PEO-based branched additive P(MMA-*r*-MnG) segregates toward the surface. This branched additive was shown by contact angle measurements to have a higher surface tension than the matrix. SANS was used to confirm its miscibility with PMMA-d_8. For blends of $\geq$2 wt % P(MMA-*r*-MnG) in PMMA-d_8, films 2000 Å thick exhibit complete coverage of the surface and silicon substrate with branched copolymer. Water absorbs into the near-surface region of these films, resulting in approximately a 30% equilibrium water content, indicative of the surfaces' hydrophilicity. Unlike PEO, P(MMA-*r*-MnG) is not water-soluble because of its PMMA content. The P(MMA-*r*-MnG)-enriched surface in blends with PMMA is consequently stable against dissolution, providing a PEO-like surface that resists protein adsorption as well as cell adhesion. This method allows, in general, for the possibility of creating high, controlled surface coverages of a higher-energy polymer additive via architectural modification. It also advances P(MMA-*r*-MnG) as a new candidate material for applications, such as biomedical implants, requiring good hydrophilicity and protein adsorption resistance.

Acknowledgment. This work was supported in part by the National Science Foundation under award No. DMR-9357602 and by the MRSEC program of the National Science Foundation under Award No. DMR-9400334. This material is also based upon activities supported by the National Science Foundation under Agreement No. DMR-9423101.

References and Notes

(1) Wu, S. *Polymer Interface and Adhesion*; Marcel Dekker: New York, 1982.
(2) Garbassi, F.; Morra, M.; Occhiello, E. *Polymer Surfaces: From Physics to Technology*; John Wiley and Sons: New York, 1994.
(3) Hariharan, A.; Kumar, S. K.; Russell, T. P. *Macromolecules* **1990**, *23*, 3584. Hariharan, A.; Kumar, S. K.; Russell, T. P. *Macromolecules* **1991**, *24*, 4909.
(4) Fredrickson, G. H.; Donley, J. P. *J. Chem. Phys.* **1992**, *97*, 8941. Wu, D. T.; Fredrickson, G. H. *J. Chem. Phys.* **1996**, *104*, 6387.
(5) Gersappe, D.; Irvine, D.; Balazs, A. C.; Liu, Y.; Sokolov, J.; Rafailovich, M.; Schwarz, S.; Peiffer, D. G. *Science* **1994**, *265*, 1072.
(6) Yethiraj, A.; Kumar, S. K.; Hariharan, A.; Schweizer, K. S. *J. Chem. Phys.* **1994**, *100*, 4691. Kumar, S. K.; Yethiraj, A.; Schweizer, K. S.; Leermakers, F. A. M. *J. Chem. Phys.* **1995**, *103*, 10332.
(7) Yethiraj, A. *Phys. Rev. Lett.* **1995**, *74*, 2018.
(8) Carignano, M. A.; Szleifer, I. *Europhys. Lett.* **1995**, *30*, 525.
(9) van der Linden, C. C.; Leermakers, F. A. M.; Fleer, G. J. *Macromolecules* **1996**, *29*, 1172.
(10) Walton, D. G.; Mayes, A. M. *Phys. Rev. E* **1996**, *54*, 2811.
(11) Wu, D. T.; Fredrickson, G. H. *Macromolecules*, **1996**, *29*, 7919.
(12) Jones, R. A. L.; Kramer, E. J.; Rafailovich, M. H.; Sokolov, J.; Schwarz, S. A. *Phys. Rev. Lett.* **1989**, *62*, 280.
(13) Steiner, U.; Klein, J.; Eiser, E.; Budkowski, A.; Fetters, L. J. *Science* **1992**, *258*, 1126.
(14) Hariharan, A.; Kumar, S. K.; Russell, T. P. *J. Chem. Phys.* **1993**, *98*, 4163.
(15) Hong, P. P.; Boerio, F. J.; Smith, S. D. *Macromolecules* **1994**, *27*, 596.

(16) Hopkinson, I.; Kiff, F. T.; Richards, R. W.; Affrossman, S.; Hartshorne, M.; Pethrick, R. A.; Munro, H.; Webster, J. R. P. *Macromolecules* **1995**, *28*, 627.
(17) Schaub, T. F.; Kellogg, G. J.; Mayes, A. M.; Kulasekere, R.; Ankner, J. F.; Kaiser, H. *Macromolecules* **1996**, *29*, 3982.
(18) Su, Z.; Wu, D.; Hsu, S. L.; McCarthy, T. J. *Macromolecules* **1997**, *30*, 840.
(19) Mayes, A. M.; Kumar S. K. *MRS Bull.* **1997**, *12*, 43.
(20) Sikka, M.; Singh, N.; Karim, A.; Bates, F. S. *Phys. Rev. Lett.* **1993**, *70*, 307.
(21) Theodorou, D. N. *Macromolecules* **1988**, *21*, 1422.
(22) Winkler, R. G.; Matsuda, T.; Yoon, D. Y. *J. Chem. Phys.* **1993**, *98*, 729.
(23) Zhao, W.; Zhao, X.; Rafailovich, M. H.; Sokolov, J.; Composto, R. J.; Smith, S. D.; Satkowski, M.; Russell, T. P.; Dozier, W. D.; Mansfield, T. *Macromolecules* **1993**, *26*, 561.
(24) Affrossman, S.; Hartshorne, M.; Jerome, R.; Pethrick, R. A.; Petitjean, S.; Rei Vilar, M. *Macromolecules* **1993**, *26*, 6251.
(25) Elman, J. F.; Johs, B. D.; Long, T. E.; Koberstein, J. T. *Macromolecules* **1994**, *27*, 5341.
(26) Harris, J. M., Ed. *Poly(ethylene glycol) Chemistry: Biotechnical and Biomedical Applications*; Plenum Press: New York, 1992.
(27) Olson, R. J.; Kaufman, H. E. In *Biocompatibility in Clinical Practice*; Williams, D. F., Ed.; CRC Press, Inc.: Boca Raton, FL, 1982; Vol. II, p 47.
(28) Olvera de la Cruz, M.; Sanchez, I. C. *Macromolecules* **1987**, *20*, 440.
(29) Shinozaki, A.; Jasnow, D.; Balazs, A. C. *Macromolecules* **1994**, *27*, 2496.
(30) Foster, D. P.; Jasnow, D.; Balazs, A. C. *Macromolecules* **1995**, *28*, 3450.
(31) Balsara, N. P.; Fetters, L. J.; Hadjichristidis, N.; Lohse, D. J.; Han, C. C.; Graessley, W. W.; Krishnamoorti, R. *Macromolecules* **1992**, *25*, 6137.
(32) Hopkinson, I.; Kiff, F. T.; Richards, R. W.; King, S. M.; Farren, T. *Polymer* **1995**, *36*, 3523.
(33) Kaiser, H.; Hamacher, K.; Kulasekere, R.; Lee, W.-T.; Ankner, J. F.; DeFacio, B.; Miceli, P.; Worcester, D. L. *Proc. SPIE-Int. Soc. Opt. Eng.* **1994**, *2241*, 78.
(34) Russell, T. P. *Mater. Sci. Rep.* **1990**, *5*, 171.
(35) Mayes, A. M.; Russell, T. P.; Satija, S. K.; Majkrzak, C. F. *Macromolecules* **1992**, *25*, 5677.
(36) Parratt, L. G. *J. Chem. Phys.* **1956**, *53*, 597.
(37) Ito, H.; Russell, T. P.; Wignall, G. D. *Macromolecules* **1987**, *20*, 2213.
(38) Hopkinson, I.; Kiff, F. T.; Richards, R. W.; Affrossman, S.; Hartshorne; Pethrick, R. A.; Munro, H.; Webster, J. R. P. *Macromolecules* **1995**, *28*, 627.
(39) Sakellariou, P. *Polymer* **1993**, *34*, 3408.
(40) Pedersen, J. S.; Hamley, I. W. *J. Appl. Crystallogr.* **1994**, *27*, 36.
(41) Zhou, X. L.; Chen, S. H. *Phys. Rep.* **1995**, *257*, 223.
(42) Data for the 2000 Å, 20% blend was taken at high resolution with an inverse geometry instead of the regular geometry used for the other samples, (*i.e.*, the incident neutrons come through the silicon substrate, hitting the silicon oxide/polymer interface first, instead of through air, hitting the air/polymer interface first) thus the dramatic increase in the oscillation amplitude from the 10% to the 20% samples.
(43) Walton, D. G., Ph.D. Thesis, MIT, Cambridge, MA, 1997.
(44) Shard, A. G.; Daview, M. C.; Tendler, S. J. B.; Nicholas, C. V.; Purbrick, M. D.; Watts, J. F. *Macromolecules* **1995**, *28*, 7855.
(45) Hoffman, A. S. *J. Biomed. Mater. Res.* **1986**, *20*, ix.
(46) Lusse, S.; Arnold, K. *Macromolecules* **1996**, *29*, 4251.
(47) Bailey, F. E., Jr.; Koleske, J. V. *Alkylene Oxides and Their Polymers*; Dekker: New York, 1991.
(48) Prime, K. L.; Whitesides, G. M. *Science* **1991**, *252*, 1164. Prime, K. L.; Whitesides, G. M. *J. Am. Chem. Soc.* **1993**, *115*, 10714.
(49) Allgor, S. J. S. Ph.D. Thesis; Massachusetts Institute of Technology: Cambridge, MA, 1996.
(50) Kenedi, R. M., Ed. *A Textbook of Biomedical Engineering*; Blackie & Son, Ltd.: Glasgow, Scotland, 1980.

MA970698+